






Design and Optimization of a Miniature Locust-Inspired Stable Jumping Robot

Yi Xu , Yanzhou Jin , Weitao Zhang, Yunhao Si, *Graduate Student Member, IEEE*, Yulai Zhang , Chang Li , and Qing Shi , *Senior Member, IEEE*

Abstract—Jumping is a key locomotion for miniature robots, but it is difficult for a robot to jump a long distance without flipping. To solve this problem, we develop a miniature locust-inspired jumping robot, which has a body length of 10 cm and weight of 60 g. On the basis of the extracted skeletal muscle movement of a locust, we make full use of the Stephenson six-bar mechanism in designing a jumping leg to achieve power amplification. Moreover, we carry out a two-step optimization of the mechanism parameters to achieve high jumping energy (first step) through optimizing the storage and dissipation of energy and then high jumping stability (second step) through optimizing the force characteristics. A series of experimental tests show that the robot can jump to a height three times its body length and a distance seven times its body length. Remarkably, the jumping height and distance relative to the body length of our jumper exceeds that of other robots with stable mechanisms by 30% and 33%, respectively. Meanwhile, our robot has a high degree of stability, which allows it to maintain a proper aerial orientation without flipping.

Index Terms—Biologically inspired robot, biomimetics, mechanism design, optimization of mechanism.

I. INTRODUCTION

DYNAMIC locomotion in complex, diverse environments has been a grand challenge in the field of miniature robotics. The locomotion of miniature robotics is usually limited to overcoming obstacles similar in size to the robot's body [1]. This phenomenon is also found in miniature animals and is known as the size–grain hypothesis; i.e., the roughness of the

Manuscript received 21 February 2023; accepted 8 June 2023. Date of current version 27 June 2023. This letter was recommended for publication by Associate Editor Y. Chen and Editor X. Liu upon evaluation of the reviewers' comments. This work was supported in part by the National Natural Science Foundation of China under Grant U2013208 and in part by the Science and Technology Innovation Program of Beijing Institute of Technology under Grant 2022CX01010. (*Corresponding author: Qing Shi.*)

Yi Xu, Yanzhou Jin, Weitao Zhang, Yunhao Si, and Qing Shi are with the Key Laboratory of Biomimetic Robots and Systems, Beijing Institute of Technology, Ministry of Education, Beijing 100081, China, and also with Intelligent Robotics Institute, School of Mechatronical Engineering, Beijing Institute of Technology, Beijing 100081, China (e-mail: 3120220160@bit.edu.cn; 1120191037@bit.edu.cn; 1120202635@bit.edu.cn; 3220210134@bit.edu.cn; shiqing@bit.edu.cn).

Yulai Zhang is with Key Laboratory of Biomimetic Robots and Systems, Beijing Institute of Technology, Beijing 100081, China, and also with the School of Medical Technology, Beijing Institute of Technology, Beijing 100081, China (e-mail: 3220215236@bit.edu.cn).

Chang Li is with Chongqing Changan Automobile, Chongqing 400021, China (e-mail: lichang3@changan.com.cn).

This letter has supplementary downloadable material available at <https://doi.org/10.1109/LRA.2023.3287795>, provided by the authors.

Digital Object Identifier 10.1109/LRA.2023.3287795

environment increases with decreasing body size, thus increasing the cost of locomotion [2]. To solve this problem, small animals, especially insects, have evolved two types of strategic locomotion, namely jumping and flying, to move efficiently across scales. In particular, jumping allows animals to move rapidly with less energy expenditure [3] and serves as a mechanism for animals to overcome obstacles, escape from predators, and capture prey. As an example, the locust adopts slow energy storage and a quick release to amplify power [4] and thus quickly jump to a safe region.

Inspired by the jumping mechanism of insects, such as locusts [5], fleas [6], and cicadas [7], scientists have made great efforts in researching jumping robots. Mirko Kovac presented a novel spherical robot that jumped up to 62 cm at a take-off angle of 75 degrees [8]. Valentin Zaitsev et al. presented a robot called TAUB, which easily reached a jumping height of 25.8 body lengths (BLs) [9]. These jumping robots overcome obstacles that are one or two orders of magnitude larger than their own height, thus achieving efficient locomotion. However, the limited ability to control the direction of the ground reaction force (GRF) and the deviation between the GRF and the jumper's center of mass (CoM) cause severe flipping during jumping [10], resulting in unpredictable landing postures. To achieve repeatable jumping, additional mechanisms, as proposed by Zhao [11] and Zhang [12], have been adopted for small-sized jumping robots to right themselves after landing, but these mechanisms make the robots heavier.

Multiple strategies have been adopted to achieve good landing postures through aerial stability: One strategy is to add wings to the robot and adopt gliding to facilitate tipping into a desirable orientation. However, the high air drag reduces the jumping height of the robot when adopting this strategy. Micro Kovac et al., for example, introduced wings to their robot and achieved jumping without flipping. However, the jump height decreased from 27 to 2.3 BLs [13], [14]. Another strategy is to carefully design the robot's mechanism and center of mass to suppress flipping during jumping, as proposed by Zhang et al. [15]. However, they did not consider the optimization of the jumping energy, and the jumping height of the robot was thus only 1 BL [16]. It is thus difficult to jump a long distance without flipping, and further studies are needed to develop miniature jumping robots having both high jumping energy and high jumping stability.

In this letter, we follow an optimization strategy and design a novel single-degree-of-freedom (SDOF) miniature jumping

robot inspired by the locust. The main contributions and novel aspects of this work relate to the design and optimization of the jumping leg to achieve long-distance and non-flipping locomotion. Experiments on a prototype robot showed that the robot hardly had any flipping motion throughout the jumping process, the orientation difference in the GRF was less than 0.14 rad, and the impulse moment in the take-off phase was approximately 0.0066 kgm²/s. Moreover, the robot achieved a jumping height of 3 BLs (30 cm) and a jumping distance of 7 BLs (70 cm). Remarkably, the jumping height and distance relative to the BL of our jumper exceeded that of other stable robots by 30% and 33%, respectively.

The remainder of this letter is organized as follows. In Section II, we analyze the jumping of a locust and propose a mechanism design for the jumping leg. In Section III, we present a two-step strategy for parameter optimization. In Section IV, we present experiments that were carried out to test the jumping performance of a prototype robot. Conclusions and future work are summarized in Section V.

II. DESIGN OF THE LOCUST-INSPIRED JUMPING LEG

In designing a miniature locust-like robot capable of jumping a long distance without flipping, we study only the musculoskeletal model of the locust, as it has the greatest effect on the jumping motion, and consider movement on a two-dimensional plane.

First, the locust jumps a long distance through power amplification, which inspires us to integrate such amplification into the robot design. Second, the stability of the locust in jumping is affected by the combined action of the front legs, jumping legs, and body, in what is a long and complex dynamic control process. However, the jumping motion actuated by the elastic energy has an extremely short duration compared with the response time of bionic systems [10], which makes it challenging for an SDOF robot to control its orientation during the take-off phase. Hence, robotics analysis and optimization are carried out in this work.

A. Analysis of the Locust Jump

A locust relies on its jumping legs in jumping, with each jumping leg mainly comprising a femur and tibia of the same length [17], [18]. According to the anatomy shown in Fig. 1, the femur has (extensor and flexor) muscles, tendons, and special tissues such as the semi-lunar process (SLP) and Heitler's lump. Specifically, the SLP acts as a spring and can stretch/contract to store/release energy [19]. Heitler's lump locks/unlocks the SLP under the control of muscles [20]. The jumping process of a locust is thus divided into three steps [21].

- 1) Co-contraction: The extensor and flexor are co-contracted to bend the SLP and thus store sufficient energy for jumping.
- 2) Unlocking: The tone of the inhibited flexor muscle falls below a threshold and the energy is released.
- 3) Jumping: Actuated by the SLP, the tibia stretches rapidly to complete the jumping process.

In the locust's jump, the tarsus plays an important role in that it fits closely with the ground and does not slip in the take-off

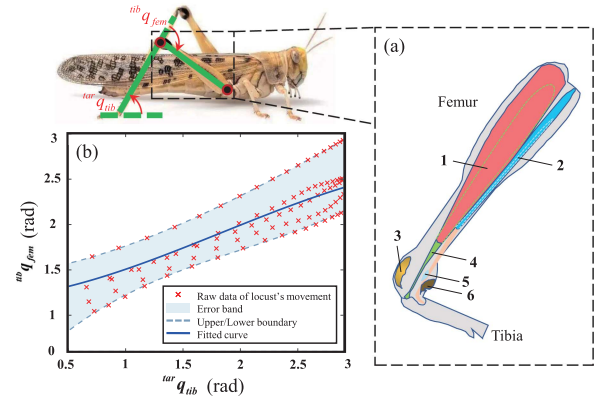


Fig. 1. Biological model: (a) Anatomy of a locust jumping leg: (1) Extensor, (2) flexor, (3) extensor tendon, (4) flexor tendon, (5) SLP, and (6) Heitler's lump; (b) the tarsus-tibia-femur relative motion model.

phase. In addition, to ensure the ideal take-off trajectory, $^{tar}q_{tib}$ (the angle between the tarsus and tibia) and $^{tib}q_{fem}$ (the angle between the tibia and femur) have a constraint relationship. We recorded a locust jumping and analyzed five non-flipping video sequences to extract movement data. We then fitted $^{tar}q_{tib}$ and $^{tib}q_{fem}$ using a three-degree polynomial, as shown in Fig. 1. The tarsus-tibia-femur relative motion model is described as follows.

$$^{tar}q_{tib} = -0.036 ^{tib}q_{fem}^3 + 0.198 ^{tib}q_{fem}^2 + 0.145 ^{tib}q_{fem} + 1.2 \quad (1)$$

On the above basis, a biomimetic jumping robot needs to follow two design rules:

- 1) The jumping motion of the robot should be similar to that of the locust, the tarsus-tibia-femur relative motion model is thus integrated into the design.
- 2) The working process of the jumping leg should involve a co-contraction mechanism for the accumulation of sufficient energy and an unlocking mechanism for releasing the stored energy rapidly.

B. Mechanism Design

In this section, we design an SDOF locust-inspired jumping leg based on a Stephenson six-bar mechanism for biomimetic jumping, as shown in Fig. 2(a). In the robot's leg, linkage BCD acts as the femur and linkage GCE acts as the tibia. A possible approach to actuating the robot is to use a driver, such as a motor working at full power, to drive the jumping leg directly. However, because of the limitations of driver technology, it is difficult to develop a miniature motor that has the same level of power density as biological muscles (over 200 W/kg [3]).

Another approach is to introduce latch-mediated spring actuation (LaMSA) [22] into the mechanism, enabling the robot to accumulate sufficient energy before jumping and releasing the energy rapidly, hence amplifying the power. To store energy, spring EI is installed between AB and GCE to imitate the SLP. When AF rotates to fold BCD and GCE , the spring is stretched, which imitates the locust's co-contraction step. When

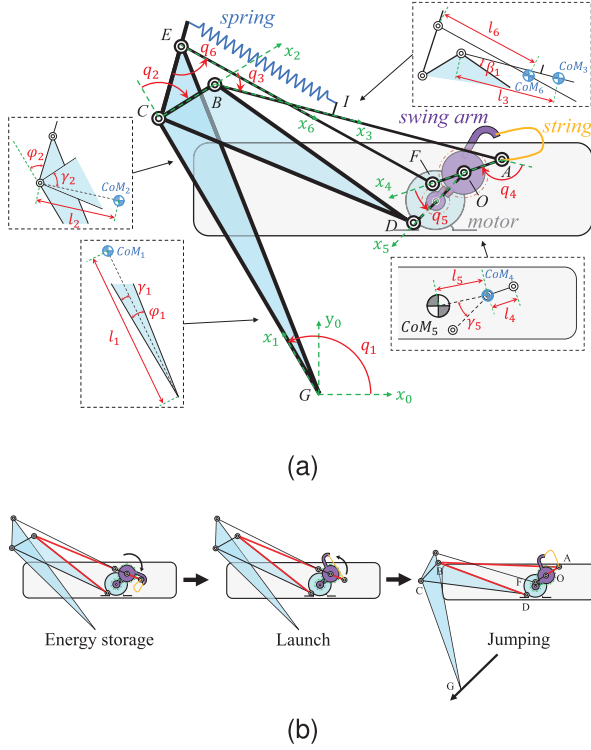


Fig. 2. Mechanism design of the robot's jumping leg: (a) SDOF robotic model and coordinate system $i, i \in \{0, 1, \dots, 6\}$; (b) working process of the jumping leg.

AF rotates in reverse, BCD and GCE expand rapidly under the actuation of the spring, providing jumping energy for the robot.

Furthermore, the SDOF jumping leg mechanism adopts an energy-locking strategy. Note that the jumping leg contains an $O - A - B - D$ crank-rocker mechanism, which is at the dead point when AF and BA are held in line. When AF and BA are pushed slightly over the dead point, there is a torque reversal at AF , but the mechanism is held in place by a contact latch [23] between AF and the body frame that locks the mechanism in place. When the motor reverses direction and the string is tightened, AF and BA are pushed over and away from the dead point, resulting in another torque reversal and thus energy releasing.

Fig. 2(b) shows that the working process of the jumping leg can be summarized as follows.

- 1) Energy storage: A motor with a gearbox drives the rocker arm to fold femur BCD and tibia GCE until the contact latch appears. The spring EI is stretched to store energy.
- 2) Launch: The motor rotates in reverse to tighten the string and thus pull AF away from the dead point to complete the launch.
- 3) Jumping: The spring actuates the jumping leg to stretch rapidly, thereby providing sufficient jumping energy.

As a result, a robot with the proposed jumping mechanism benefits from LaMSA and hence achieves power amplification. It is worth noting that the working process of the jumping leg

is largely similar to that of a locust and follows the design rules summarized in Section II-A. Our leg mechanism is thus biomimetic.

C. Kinematic Analysis

To obtain the relationship between the movement trajectory of CoM_5 and q_5 (the angle of AF relative to the body), we analyze the kinematics of the leg mechanism. As shown in Fig. 2(a), we first set up a world coordinate system $x_0 - G - y_0$ with the origin fixed on G and the x_0 -axis directed horizontally. We then analyze the kinematics on the basis of three vector loops and expand them using the Euler formula

$$l_{BA} \cdot e^{i0} + l_{AO} \cdot e^{iq_4} + l_{OD} \cdot e^{i(q_4 - q_5)} = l_{BD} \cdot e^{i\beta_1} \quad (2)$$

$$l_{CB} \cdot e^{i0} + l_{BA} \cdot e^{iq_3} + l_{AO} \cdot e^{i(q_3 + q_4)} + l_{OD} \cdot e^{i(q_3 + q_4 - q_5)} = l_{CD} \cdot e^{i\angle BCD} \quad (3)$$

$$l_{CB} \cdot e^{i(q_2 - \varphi_2)} + l_{BA} \cdot e^{i(q_2 - \varphi_2 + q_3)} + l_{AF} \cdot e^{i(q_2 - \varphi_2 + q_3 + q_4)} = l_{CE} \cdot e^{i0} + l_{EF} \cdot e^{i(\pi - q_6)} \quad (4)$$

where l_{wz} is the length of linkage wz , q_1 is the angle between GC and the x -axis, and q_i is the relative angle between two adjacent linkages, $w \& z \in \{A, B, C, D, E, F, G, H, O\}$, $i \in \{2, 3, 4, 6\}$.

The rotating joint G has a passive degree of freedom, and its movement is thus not subject to any constraint. We use the tarsus-tibia-femur relative motion model fitted with biological data in Section II-A to constrain q_1 , where $^{tar}q_{tib}$ is replaced by q_1 and $^{tib}q_{fem}$ by $(q_2 + q_3)$.

D. Dynamic Analysis

In an actual jumping motion, the mass properties of the robot and the position of the CoM directly affect the robot's jumping stability. We thus assign mass properties to the robot and establish a passive jumping dynamic model. Here, we assume that: 1) the foot and ground are in rigid contact with no elastic deformation; 2) the point G does not slide relative to the ground when the robot takes off. Hence, the point G is simplified as a plane hinge, and the tibia rotates around the axis of G .

The dynamic model of the locust-inspired robot is shown in Fig. 2(a) and definitions are given as follows. The center of mass of each (triangular) linkage in the leg is CoM_i , the length from the center of mass to the end of the previous linkage is l_i , the mass is m_i , and the rotational inertia relative to the center of mass is I_i (around the z -axis, perpendicular to the plane of the paper). In particular, the body is represented by a rectangle whose mass is centered on CoM_5 .

First, we analyze the energy for each part. When analyzing the elastic potential energy of the spring, we calculate the length of the spring according to the mounting points E and I at the two ends, using 0T_E and 0T_I . The total kinetic energy and potential energy of the system are

$$\begin{cases} E_k = \sum_{i=1}^6 E_{k_i} = \sum_{i=1}^6 \left(\frac{1}{2} m_i v_{CoM_i}^2 + \frac{1}{2} I_i \omega_i^2 \right) \\ E_P = \sum_{i=1}^6 (m_i g h_i) + \frac{1}{2} k (l_k^2(q_5) - L_0^2) \end{cases} \quad (5)$$

where

$$l_k(q_5) = \sqrt{\left[({}^0T_E - {}^0T_I)^2\right]_{(4,1)} + \left[({}^0T_E - {}^0T_I)^2\right]_{(4,2)}} \quad (6)$$

where 0T_E is a 4×4 homogeneous transformation matrix and point E is expressed in the world coordinate system 0. We next apply the above formula to Lagrange's dynamical equations and derive the generalized coordinates to obtain the motion equation of the robot

$$\frac{d}{dt} \left(\frac{\partial E_K}{\partial \dot{q}_5} \right) - \frac{\partial E_K}{\partial q_5} + \frac{\partial E_P}{\partial q_5} = 0 \quad (7)$$

Finally, we consider the aerial phase, in which the launch energy of the robot is lost through air drag. As a matter of fact, the stored elastic energy has converted into the launch energy at the end of the take-off phase and the robot has fully stretched and can be regarded as a rigid body. The dynamic equations of the aerial phase are

$$\ddot{x} = \frac{F_{drag} \cos \theta_{pitch}}{m_{rob}} \quad (8)$$

$$\ddot{y} = \frac{F_{drag} \sin \theta_{pitch} + mg}{m_{rob}} \quad (9)$$

$$\ddot{\theta}_{pitch} = \frac{(F_{drag} + mg \sin \theta_{pitch}) \cdot {}^5l_y - mg \cos \theta_{pitch} \cdot {}^5l_x}{I_{rob}} \quad (10)$$

and the air drag can be given by

$$F_{drag} = \frac{1}{2} \rho S (x^2 + y^2) C_D(\theta_{pitch}) \quad (11)$$

where m_{rob} and I_{rob} are the mass and rotational inertia of the robot, ρ is the air density, S is the projected area of the robot in the direction of motion relative to the air, v is the velocity relative to the air, $({}^5l_x, {}^5l_y)$ is the actual position of the robot's CoM relative to CoM_5 , C_D is the drag coefficient, and θ_{pitch} is the orientation angle of the robot relative to the horizontal ground.

III. OPTIMIZATION OF MECHANISM PARAMETERS

A. First Step: Optimization of the Jumping Energy

The first optimization objective is the jumping energy of the robot. To achieve a long-distance jumping motion, the robot needs to store enough energy within the allowable range of the motor torque. Moreover, it is important to reduce energy dissipation during the take-off phase.

It is worth noting that when storing the same energy, the optimized spring stroke will have a lower requirement for the spring stiffness coefficient k , which will lead to a lower torque requirement for the motor. We therefore optimize the spring stroke through the variable λ to store more elastic potential energy. The kinematic model shows that the truss GCE has the largest rotation angle relative to the linkage AB in the take-off phase, and the stroke is a maximum when the two ends of the spring are installed on these two linkages. Therefore, λ should

be determined to satisfy

$$\max f_1 = \left[(x_E - x_I)^2 + (y_E - y_I)^2 \right]_{step=n} - \left[(x_E - x_I)^2 + (y_E - y_I)^2 \right]_{step=1} \quad (12)$$

where n is the total number of optimization steps. ${}^{i-1}T_i (i \in \{1, 2, 3, 4, 5\})$ is the transformation matrix of coordinate system i and coordinate system $i - 1$:

$$\begin{cases} x_E = [{}^0T_1 \cdot {}^1T_E]_{(4,1)} \\ y_E = [{}^0T_1 \cdot {}^1T_E]_{(4,2)} \end{cases} \quad (13)$$

$$\begin{cases} x_I = \left[\left(\prod_{i=1}^3 {}^{i-1}T_i \right) \cdot {}^3T_I \right]_{(4,1)} \\ y_I = \left[\left(\prod_{i=1}^3 {}^{i-1}T_i \right) \cdot {}^3T_I \right]_{(4,2)} \end{cases} \quad (14)$$

$${}^3T_I = \begin{bmatrix} 1 & 0 & 0 & \lambda \cdot l_{BA} \\ 0 & 1 & 0 & 0 \\ 0 & 0 & 1 & 0 \\ 0 & 0 & 0 & 1 \end{bmatrix} \quad (15)$$

We observe that when the locust takes off, the trajectory of its body's center of mass is approximately linear, so that energy dissipation is reduced in normal motion. We thus first set the two optimization variables γ_5 and l_5 to find the best position of CoM_5 . We discretize the motion interval of q_5 and obtain n discrete points on the motion trajectory of CoM_5 according to the kinematic relationship. In ensuring linearity, γ_5 and l_5 are determined to satisfy

$$\min f_2 = \sum_{step=2}^{n-1} \left| \frac{y_{CoM_5}^{step+1} - y_{CoM_5}^{step}}{x_{CoM_5}^{step+1} - x_{CoM_5}^{step}} - \frac{y_{CoM_5}^{step} - y_{CoM_5}^{step-1}}{x_{CoM_5}^{step} - x_{CoM_5}^{step-1}} \right| \quad (16)$$

where the position of CoM_5 in the world coordinate system $x - G - y$ can be represented by (x_{CoM_5}, y_{CoM_5}) :

$$\begin{cases} x_{CoM_5}(q_5) = \left[\left(\prod_{i=1}^5 {}^{i-1}T_i(q_5) \right) \cdot {}^5T_{CoM_5} \right]_{(4,1)} \\ y_{CoM_5}(q_5) = \left[\left(\prod_{i=1}^5 {}^{i-1}T_i(q_5) \right) \cdot {}^5T_{CoM_5} \right]_{(4,2)} \end{cases} \quad (17)$$

$${}^5T_{CoM_5} = \begin{bmatrix} c_{\gamma_5} & -s_{\gamma_5} & 0 & l_5 \\ s_{\gamma_5} & c_{\gamma_5} & 0 & 0 \\ 0 & 0 & 1 & 0 \\ 0 & 0 & 0 & 1 \end{bmatrix} \quad (18)$$

B. Second Step: Optimization of the Jumping Stability

The second optimization objective is the jumping stability of the robot. Considering that most of the mass of the robot is concentrated in the body part, it is sound to analyze the flipping effect at CoM_5 instead of the stress point G . We consider 1) whether the orientation of the translated force acting on CoM_5 is invariant, leading to a clear direction of the acceleration, and 2) whether the generated torque has a stable effect on CoM_5 , preventing the robot from flipping appreciably.

In Section III-A, there is an implicit premise that the optimization is performed under specific linkage lengths when searching for the best position of CoM_5 , and it is thus noted that the lengths of linkages are important optimization variables. Under the premise of a certain material density, the mass properties of the linkage, including the mass, rotational inertia, and location of the center of mass, will change as a linkage length changes, which will affect the force characteristics of the robot. We therefore select the lengths of the different linkages as the optimization variables:

$$X = \begin{bmatrix} l_{BA} & l_{AO} & l_{OD} & l_{BD} & l_{CB} & l_{CD} \\ l_{AF} & l_{CE} & l_{EF} & l_{GC} & l_{GE} & l_{DH} \end{bmatrix}$$

We then use the Newton–Euler equations to deduce the inertial force and inertial moment of each part of the robot. We want the orientation of the inertial force to be as consistent as possible, and the accumulation of the inertial moment during the take-off stage to be as small as possible:

$$\min f_3 = \sum_{step=2}^{n-1} \left| \tan^{-1} \frac{{}^0F_{I_{5y}}^{step}}{{}^0F_{I_{5x}}^{step}} - \tan^{-1} \frac{{}^0F_{I_{5y}}^{step-1}}{{}^0F_{I_{5x}}^{step-1}} \right| \quad (19)$$

$$\min f_4 = \sum_{step=1}^n {}^0M_{I_5}^{step} \cdot \Delta t \quad (20)$$

Newton–Euler equations establish the relationship between the motion and force. In the optimization of objectives f_3 and f_4 , the inertial force and inertial moment during the take-off phase are calculated as

$$\begin{cases} {}^0F_{I_5} = \prod_{i=1}^5 {}^{i-1}R_i (m_5 \cdot {}^5\dot{v}_{CoM_5}) \\ {}^0M_{I_5} = \prod_{i=1}^5 {}^{i-1}R_i (I_5 \cdot {}^5\dot{\omega}_5 + {}^5\omega_5 \times I_5 \cdot {}^5\omega_5) \end{cases} \quad (21)$$

where ${}^0F_{I_5}$ is the inertial force acting on the body, ${}^0M_{I_5}$ is the inertial moment, ${}^i\dot{v}_{CoM_i}$ is the acceleration, ${}^i\dot{\omega}_i$ is the angular acceleration, ${}^i\omega_i$ is the angular velocity, and ${}^{i-1}R_i$ is the matrix of rotation between coordinate system i and coordinate system $i-1$.

There are quite a few variables in the optimization, resulting in a large search domain in the solution space. Hence, reasonable constraints need to be set to narrow the domain. First, the optimization needs to meet physical conditions, including the length of each linkage being larger than zero and the triangular condition of truss GCE and truss BCD .

The anatomy of the locust's jumping leg shows that the length ratio of the femur and tibia is approximately 1 : 1 [24]. By setting ϵ_1 and ϵ_2 to no more than 0.5, we introduce this biometric feature into the bionic constraints of the robot's jumping leg. In addition to the length limit, the angle between the femur and tibia is small before the locust takes off, and the robot limits this angle to $q_2 + q_3$. We thus have

$$\begin{cases} l_{EF} = l_{CD} + \epsilon_1 \\ l_{CG} = l_{CD} + \epsilon_2 \\ 0 < [q_2 + q_3]_{(step=1)} \leq \frac{\pi}{6} \end{cases} \quad (22)$$

Finally, it is necessary to define the moment when the robot leaves the ground. On the one hand, the robot leaves the ground

TABLE I
GLOBAL OPTIMAL SOLUTION OF LINKAGE LENGTHS

linkage	OR	linkage	OR	linkage	OR
l_{BA}	58.1396	l_{CD}	66.8002	l_{GE}	68.0077
l_{AO}	5.3234	l_{AF}	10.8551	l_{DH}	2.7761
l_{OD}	13.7222	l_{CE}	14.6428	l_5	0.01
l_{BD}	61.1218	l_{EF}	60.6096	γ_5	1.5708
l_{CB}	7.6529	l_{GC}	59.1005	λ	0.19

when its jumping leg fully stretches, which can be introduced by the vertical reaction force ${}^0F_{I_{5y}}^{step}$ goes to zero. On the other hand, when the robot's feet slip, the horizontal force changes from static friction to sliding friction. In this case, the value of ${}^0F_{I_{5x}}^{step}$ will suddenly decreases. The leaving moment $flag_{jump}$ can be described as

$$flag_{jump} = \begin{cases} 1, & ({}^0F_{I_{5y}}^{step} = 0) \text{ or } ({}^0F_{I_{5x}}^{step} \ll {}^0F_{I_{5x}}^{step-1}) \\ 0, & \text{otherwise} \end{cases} \quad (23)$$

C. Optimization Results

In this work, the first step of optimizing the jumping energy has two separate objectives, f_1 and f_2 , which can be solved through particle swarm optimization. Meanwhile, the second step of optimizing the jumping stability has two related objectives, f_3 and f_4 , which can be solved through multi-objective optimization. We thus adopt a multi-objective particle swarm optimization algorithm. For both steps of optimization, we set the population $n_p = 5$ and the iteration number $n_I = 10$. The optimal results (OR) are given in Table I.

In the first step of optimization, we define the normalized objective function score by ${}^1f_{stp1}^{norm}$ and ${}^2f_{stp1}^{norm}$. As shown in Fig. 3(a), the maximum spring stroke (red circle) and the best score ${}^1f_{stp1}^{norm}$ (the top gray circle in each blue box) increase with n_I . Then, we calculate the RMSE of the CoM_5 trajectory's linear fitting. As shown in Fig. 3(b), the minimum RMSE in each swarm and the best score ${}^2f_{stp1}^{norm}$ (the bottom gray circle in each blue box) decrease with n_I . Finally, the optimal stroke of the spring is 15 mm and the theoretical maximum stiffness coefficient of the spring is 5534.96 N/m within the permissible torque range of the motor, which achieves energy accumulation of 0.41 J. The high linearity of the trajectory of CoM_5 leads to almost no energy dissipation in the normal motion. In this case, the robot achieves a jumping motion that is 90 cm long and 40 cm high when the initial take-off angle is 60 deg.

$$\begin{cases} {}^1f_{stp1}^{norm} = \frac{f_1}{\max[f_1]_{(n_I=1)}} \\ {}^2f_{stp1}^{norm} = \frac{f_2}{\max[f_2]_{(n_I=1)}} \end{cases} \quad (24)$$

In the second step of optimization, each particle represents a group of linkage lengths of the jumping leg mechanism, and the normalized objective function score f_{stp2}^{norm} is determined as follows (where α_1, α_2 are set as 0.5) and decreases with n_I as shown in the black box of Fig. 4. In the optimization, there are a total of 50 particles, the inertial force and inertial moment of which are calculated for comparison of the jumping stability. The mechanism represented by the worst particle in the first

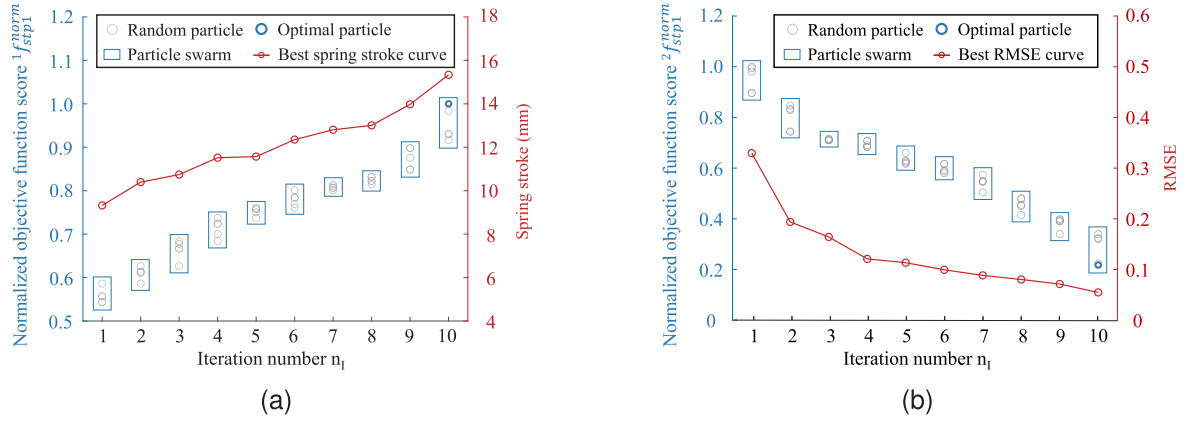


Fig. 3. 1st step optimization result: (a) Optimization on the spring stroke; (b) optimization on the position of CoM_5 .

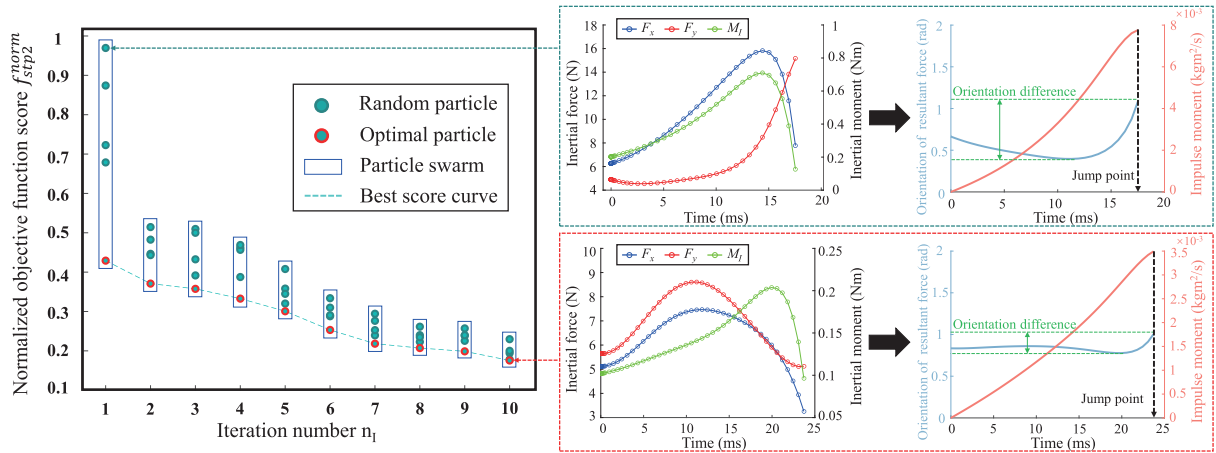


Fig. 4. 2nd step optimization result: (a) black box: the normalized objective score of each particle in the optimization process; (b) green box: force characteristics of the worst particle in the first iteration; (c) red box: force characteristics of the best particle in the last iteration.

iteration (green box) and the best particle in the last iteration (red box) are shown on the right of Fig. 4. It is seen that the orientation difference of the inertial force is 0.7011 rad and the impulse moment is $0.0078 \text{ kgm}^2/\text{s}$ for the green box, whereas the orientation difference is 0.2274 rad and impulse moment is $0.0035 \text{ kgm}^2/\text{s}$ for the red box. In summary, the orientation change of the inertia force drops by 67.6% and the impulse moment drops by 55.1%, which means that the jumping stability improves.

$$f_{stp2}^{norm} = \frac{\alpha_1 \cdot f_3}{\max[f_3]_{(Iteration=1)}} + \frac{\alpha_2 \cdot f_4}{\max[f_4]_{(Iteration=1)}} \quad (25)$$

IV. EXPERIMENTS AND ANALYSIS

A. Experimental Setup

The overall design of the miniature locust-inspired jumping robot is shown in Fig. 5(a). The design has a length of 10 cm and a height of 8 cm. Using three-dimensional printing technology, we developed a lightweight prototype with a total mass of 60 g,

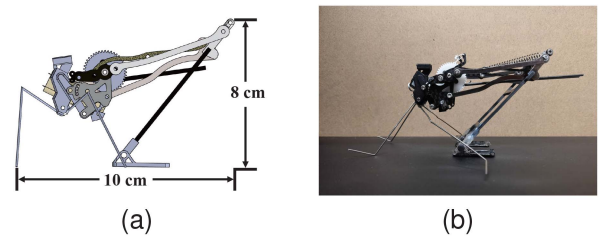


Fig. 5. 3-D model and prototype of the locust-inspired robot: (a) 3-D model of the locust-inspired robot; (b) prototype of the locust-inspired robot using in the following experiments.

as shown in Fig. 5(b). Owing to the symmetrical structure of the robot, we studied its movement only on a two-dimensional plane. To capture the real-time position and orientation of the robot throughout the jumping process, we set three markers on the head, center of mass, and rear end of the robot.

The experimental setup mainly included the prototype of the proposed robot, a DC power supply, a customized force plate (NBIT GF 2410, used in recent research on a robotic rat [25]),

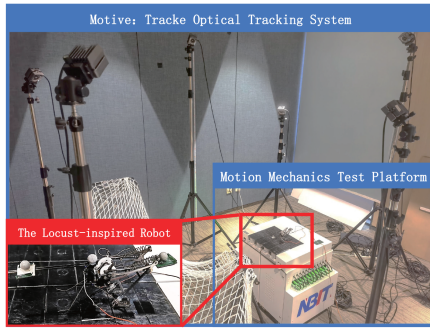


Fig. 6. Experimental site for the small-sized locust-inspired robot, including a prototype of the proposed robot, a customized force plate and a standard optical tracking system.

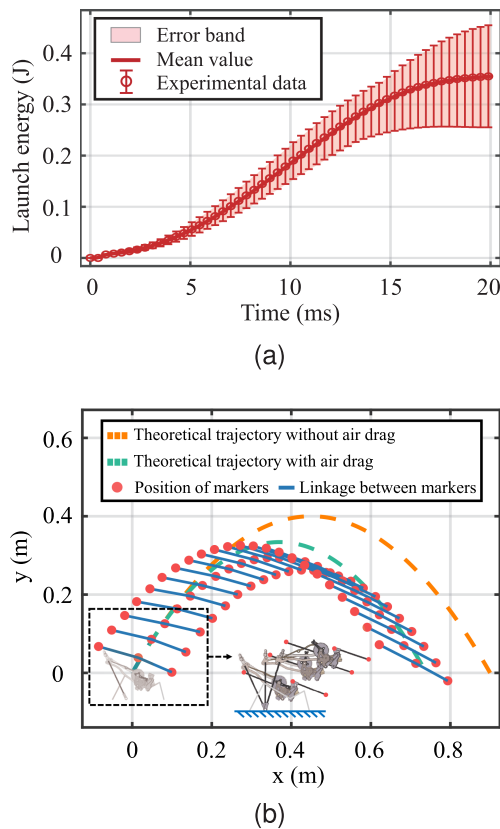


Fig. 7. Long-distance jumping tests: (a) Experimental data of the robot's launch energy; (b) theoretical and experimental trajectory of the locust-inspired robot in the whole jumping process.

and a standard optical tracking system (Motive: Tracker), as shown in Fig. 6.

B. Long-Distance Jumping Tests

To evaluate the jumping performance of the proposed robot, we captured movement data of the robot using a standard optical tracking system and calculated the kinetic energy using the frame difference method [29], as shown in Fig. 7(a). Within 20 ms, the robot accelerated appreciably and completed the launch process. The mean value of the launch energy was approximately 0.36 J in the take-off phase, which agreed the theoretical maximum

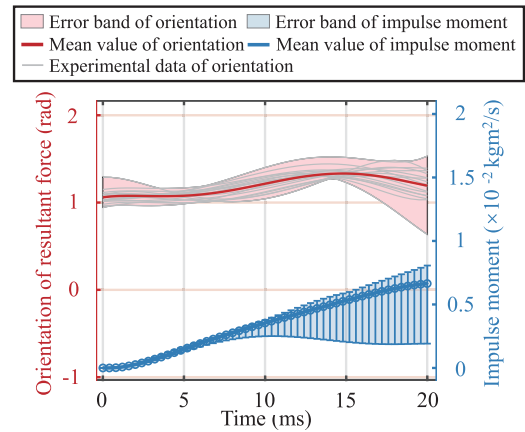


Fig. 8. Non-flipping jumping tests, including the orientation of the resultant force acting on the robot feet and the experimental data of the impulse moment in the take-off phase.

storable energy (0.41 J) obtained in Section III-C. One of the best jumping performances of the robot is shown in Fig. 7(b). The position of the robot was recorded using the marker on the robot's center of mass, and the orientation using the markers on the head and rear end. It is seen that the robot was able to jump with a fully extended posture, to a maximum height of 30 cm and a maximum distance of 70 cm. At the end of the aerial phase, the energy of the robot decreased to 0.32 J and the 11% energy loss was due to air drag.

Compared with existing stable miniature jumping robots having a maximum jumping height of 2.1 BLs and maximum jumping distance of 4.7 BLs, our robot has considerable advantages as shown in Table II. Remarkably, the jumping height and distance relative to the BL of our jumper exceeded that of the other robots by 30% and 33%, respectively.

C. Non-Flipping Jumping Tests

To characterize the stability of the external force acting on the robot, we measured the GRF using the customized force plate and calculated the orientation of the resultant force, as shown in Fig. 8. It is seen that the mean orientation of the resultant force fluctuated in a small range around 1.2 rad and the orientation difference did not exceed 0.14 rad. As a result, the orientation of the external force acting on the robot feet fluctuated in a small range during the take-off phase, providing the foundation for the jumping stability of the robot. Moreover, we calculated the impulse moment acting on the robot by integrating the torque with time. The mean value was $0.0066 \text{ kgm}^2/\text{s}$, which was consistent with the theoretical calculated value, and the resulting angular velocity was 0.2 rad/s.

As shown in Fig. 7(b), the difference in the jumping orientation between the initial pose and end pose was approximately 4 deg, which was less than that for the other robots in Table II. Furthermore, the optimization of the jumping stability in Section III-B only concentrates on the GRF related to the robot's CoM. Hence the pre-optimized robot was even capable of stable jumping from an inclined surface (as shown in the video).

TABLE II
COMPARISON OF STATE-OF-THE-ART ROBOTS' JUMPING PERFORMANCE AND STABILITY

Robot	Mass	Boby Length	Jumping Height	Jumping Distance	Jumping orientation difference
Yin <i>et al</i> [26]	108 g	> 10.0 cm	21.2 cm (2.1 BL)	NA	NA
Li <i>et al</i> [27]	22 g	5.0 cm	NA	20.0 cm (4 BL)	< 5 deg (high stability)
Chen <i>et al</i> [28]	30 g	7.8 cm	16.0 cm (2.1 BL)	25.0 cm (3.2 BL)	< 45 deg (low stability)
Zhang <i>et al</i> [16]	229 g	25.3 cm	34.0 cm (1.3 BL)	120.0 cm (4.7 BL)	32.19 deg (low stability)
This work	60 g	10.0 cm	30.0 cm (3.0 BL)	70.0 cm (7.0 BL)	4 deg (high stability)

V. CONCLUSION

Achieving both high degrees of ability and stability is an important step in the practical application of miniature jumping robots. In this study, we first analyzed captured data of a locust and established a tarsus–tibia–femur relative motion model. We then made full use of a SDOF Stephenson six-bar mechanism to design the jumping leg for a robot and optimized its mechanism parameters, thus improving both the jumping energy and jumping stability. Finally, we built a physical prototype to show that the optimized robot was capable of both long-distance and non-flipping jumping motion. The results obtained in field tests showed that the robot achieved a jump height of 3 BLs (30 cm) and a jump distance of 7 BLs (70 cm), with the difference in orientation between the initial pose and end pose being approximately 4 deg.

We demonstrated that the proposed jumping strategy achieved excellent jumping performance and that it has great potential in practical applications. In future research, we will use the characteristics of stable jumping combined with flying to improve the moving range of the robot.

REFERENCES

- [1] R. Armour, K. Paskins, A. Bowyer, J. Vincent, and W. Megill, "Jumping robots: A biomimetic solution to locomotion across rough terrain," *Bioinspiration Biomimetics*, vol. 2, no. 3, pp. S65–S82, Sep. 2007, doi: [10.1088/1748-3182/2/3/S01](https://doi.org/10.1088/1748-3182/2/3/S01).
- [2] M. Kaspari and M. D. Weiser, "The size–grain hypothesis and interspecific scaling in ants," *Funct. Ecol.*, vol. 13, no. 4, pp. 530–538, Aug. 1999, doi: [10.1046/j.1365-2435.1999.00343.x](https://doi.org/10.1046/j.1365-2435.1999.00343.x).
- [3] U. B. Hanan, A. Weiss, and V. Zaitsev, "Jumping efficiency of small creatures and its applicability in robotics," *Procedia Manuf.*, vol. 21, pp. 243–250, 2018. [Online]. Available: <https://linkinghub.elsevier.com/retrieve/pii/S2351978918301525>
- [4] H. Bennet-Clark, "The energetics of the jump of the locust *Schistocerca gregaria*," *J. Exp. Biol.*, vol. 63, no. 1, pp. 53–83, 1975.
- [5] V. Zaitsev, O. Gvirsman, U. B. Hanan, A. Weiss, and G. Kosa, "Locust-inspired miniature jumping robot," in *Proc. IEEE/RSJ Int. Conf. Intell. Robots Syst.*, 2015, pp. 553–558.
- [6] M. D. Christie, S. S. Sun, D. H. Ning, H. Du, S. W. Zhang, and W. H. Li, "A torsional MRE joint for a C-shaped robotic leg," *Smart Mater. Struct.*, vol. 26, no. 1, Nov. 2016, Art. no. 015002, doi: [10.1088/0964-1726/26/1/015002](https://doi.org/10.1088/0964-1726/26/1/015002).
- [7] U. Scarfogliero, F. Li, D. Chen, C. Stefanini, W. Liu, and P. Dario, "Jumping mini-robot as a model of scale effects on legged locomotion," in *Proc. IEEE Int. Conf. Robot. Biomimetics*, 2007, pp. 853–858.
- [8] M. Kovač, M. Schlegel, J. C. Zufferey, and D. Floreano, "Steerable miniature jumping robot," *Auton. Robots*, vol. 28, no. 3, pp. 295–306, 2010.
- [9] V. Zaitsev, O. Gvirsman, U. B. Hanan, A. Weiss, A. Ayali, and G. Kosa, "A locust-inspired miniature jumping robot," *Bioinspiration Biomimetics*, vol. 10, no. 6, Nov. 2015, Art. no. 066012, doi: [10.1088/1748-3190/10/6/066012](https://doi.org/10.1088/1748-3190/10/6/066012).
- [10] G. Ribak, "Insect-inspired jumping robots: Challenges and solutions to jump stability," *Curr. Opin. Insect Sci.*, vol. 42, pp. 32–38, 2020. [Online]. Available: <https://www.sciencedirect.com/science/article/pii/S2214574520301097>
- [11] J. Zhao et al., "MSU jumper: A single-motor-actuated miniature steerable jumping robot," *IEEE Trans. Robot.*, vol. 29, no. 3, pp. 602–614, Jun. 2013.
- [12] J. Zhang, G. Song, Z. Li, G. Qiao, H. Sun, and A. Song, "Self-righting, steering and takeoff angle adjusting for a jumping robot," in *Proc. IEEE/RSJ Int. Conf. Intell. Robots Syst.*, 2012, pp. 2089–2094.
- [13] M. Kovac, M. Fuchs, A. Guignard, J.-C. Zufferey, and D. Floreano, "A miniature 7G jumping robot," in *Proc. IEEE Int. Conf. Robot. Automat.*, 2008, pp. 373–378.
- [14] M. Kovac, Wassim-Hraiz, O. Fauria, J.-C. Zufferey, and D. Floreano, "The EPFL jumpglider: A hybrid jumping and gliding robot with rigid or folding wings," in *Proc. IEEE Int. Conf. Robot. Biomimetics*, 2011, pp. 1503–1508. [Online]. Available: <https://ieeexplore.ieee.org/document/6181502/>
- [15] Z. Zhang et al., "Mechanism design for locust-inspired robot with one-DOF leg based on jumping stability," *Mechanism Mach. Theory*, vol. 133, pp. 584–605, Mar. 2019. [Online]. Available: <https://linkinghub.elsevier.com/retrieve/pii/S0094114X18316410>
- [16] Z. Zhang, B. Chang, J. Zhao, Q. Yang, and X. Liu, "Design, optimization, and experiment on a bioinspired jumping robot with a six-bar leg mechanism based on jumping stability," *Math. Problems Eng.*, vol. 2020, pp. 1–23, Jan. 2020. [Online]. Available: <https://www.hindawi.com/journals/mpe/2020/3507203/>
- [17] C. Yong, "Biological mechanism of the locust jumping robot," in *Proc. Int. Conf. Elect. Control Eng.*, Wuhan, China, 2010, pp. 2676–2679. [Online]. Available: <https://ieeexplore.ieee.org/document/5630623/>
- [18] W. J. Heitler, "The Locust Jump: III. Structural specializations of the metathoracic tibiae," *J. Exp. Biol.*, vol. 67, no. 1, pp. 29–36, 1977. [Online]. Available: <https://www.mendeley.com/catalogue/8de0142e-7fe8-359f-8977-554ed7c6c5a5/>
- [19] C. Wan, Z. Hao, and S. N. Gorb, "Time-scale mechanical behaviors of locust semi-lunar process cuticles under power amplification for rapid movements," *J. Biomech.*, vol. 104, May 2020, Art. no. 109742. [Online]. Available: <https://linkinghub.elsevier.com/retrieve/pii/S0021929020301585>
- [20] Y. Geng, Z. Yang, and F. Lin, "Optimization of dual side control strategy for wireless power transfer system in light rail vehicle," in *Proc. IEEE PELS Workshop Emerg. Technol.: Wireless Power Transfer*, 2016, pp. 54–59. [Online]. Available: <https://ieeexplore.ieee.org/document/7772066/>
- [21] W. J. Heitler and M. Burrows, "The locust jump. I. The motor programme," *J. Exp. Biol.*, vol. 66, no. 1, pp. 203–219, Feb. 1977.
- [22] S. Longo et al., "Beyond power amplification: Latch-mediated spring actuation is an emerging framework for the study of diverse elastic systems," *J. Exp. Biol.*, vol. 222, no. 15, 2019, Art. no. jeb197889.
- [23] M. Ilton et al., "The principles of cascading power limits in small, fast biological and engineered systems," *Science*, vol. 360, no. 6387, 2018, Art. no. eaao1082.
- [24] M. A. Woodward and M. Sitti, "Morphological intelligence counters foot slipping in the desert locust and dynamic robots," *Proc. Nat. Acad. Sci. USA*, vol. 115, no. 36, pp. E8358–E8367, Sep. 2018, doi: [10.1073/pnas.1804239115](https://doi.org/10.1073/pnas.1804239115).
- [25] Q. Shi et al., "Development of a small-sized quadruped robotic rat capable of multimodal motions," *IEEE Trans. Robot.*, vol. 38, no. 5, pp. 3027–3043, Oct. 2022.
- [26] X. Yin, J. Yan, S. Wen, and J. Zhang, "Spring-linkage integrated mechanism design for jumping robots," *Robot. Auton. Syst.*, vol. 158, 2022, Art. no. 104268. [Online]. Available: <https://www.sciencedirect.com/science/article/pii/S0921889022001579>
- [27] F. Li et al., "Jumping like an insect: Design and dynamic optimization of a jumping mini robot based on bio-mimetic inspiration," *Mechatronics*, vol. 22, no. 2, pp. 167–176, 2012. [Online]. Available: <https://www.sciencedirect.com/science/article/pii/S0957415812000025>
- [28] K. Chen, D. Chen, Z. Zhang, and M. Wang, "Jumping robot with initial body posture adjustment and a self-righting mechanism," *Int. J. Adv. Robot. Syst.*, vol. 13, no. 3, 2016, Art. no. 127, doi: [10.5772/64200](https://doi.org/10.5772/64200).
- [29] N. Singla, "Motion detection based on frame difference method," *Int. J. Inf. Computation Technol.*, vol. 4, pp. 1559–1565, 2014.